Results in Engineering 23 (2024) 102535

Contents lists available at ScienceDirect

Results in Engineering

journal homepage: www.sciencedirect.com/journal/results-in-engineering

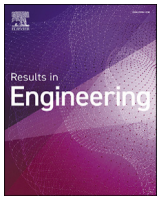

Research paper

Transition from laminar to turbulent pipe flow as a process of growing material instabilities

Saptarshi Kumar Lahiri [*,1], Konstantin Volokh [1]

Technion Israel Institute of Technology, Faculty of Civil and Environmental Engineering, Haifa, 3200003, Israel

ARTICLE INFO

Keywords:
Transition into turbulence
Viscous strength model
Pipe flow simulation
Navier-Stokes model

ABSTRACT

Experiments show that a laminar pipe flow starts to change to turbulence at Reynolds numbers around 2000. However, the classical Navier-Stokes theory fails to explain such a transition; according to it the pipe flow should always be stable and laminar. In the present work, it is hypothesized that the transition to turbulence occurs due to material rather than kinematic instabilities of the flow, and the classical Navier-Stokes theory is enhanced with a description of viscous strength. Numerical simulations of the pipe flow with and without the viscous strength are performed. The results show that material instabilities due to the viscous strength gradually develop into a turbulent flow, in agreement with the experimental observations. In the absence of viscous strength, the pipe flow remains laminar in disagreement with experiments. It is concluded that the material instabilities can generally compete with the kinematic ones in the process of transition from laminar to turbulent flow.

1. Introduction

Considering pipe flow, Osborne Reynolds [1,2] introduced a non-dimensional parameter $Re = \rho v D/\eta$, in which ρ is the mass density of the fluid, v is the mean velocity, D is the diameter of the pipe, and η is the viscosity of the fluid. Reynolds assumed that the transition from laminar to turbulent flow occurred at some critical number Re_{cr}. Experimental estimates of this critical number for water vary from 1700 and 2300 [3,4] to 3000 [5]. Recently, Avila et al. [6] experimentally studied laminar flow through a 15 m long pipe with a diameter of 4 mm and observed that at $Re_{cr} \approx 2400$ the laminar flow became unstable and indicated transition to turbulence.

Theoretical explanations of the transition to turbulence have a long history [7–15] and debates proceed nowadays. Unfortunately, the linear instability analysis cannot capture the onset of failure of the laminar flow, which is observed in experiments. The linear instability analysis tracks the evolution of infinitesimal or small perturbations, e.g., molecular fluctuations, which always exist. Such perturbations do not develop into transitional flow according to the Navier-Stokes theory [16,17].

To accommodate the experimentally observed transition to turbulence within the framework of the Navier-Stokes theory, some authors assume the existence of finite or large perturbations in the laminar flow [4,5,18]. Numerous numerical studies [19–26] have simulated pipe floes and have observed that increasing the Reynolds number (Re) leads to turbulence in pipe flow, regardless of the magnitude of local perturbations. These perturbations were primarily attributed to background distortions and numerical noise, which trigger turbulence. Luciano [26] recently noted that to accurately simulate and generate turbulence in the flow, it is essential to manually introduce perturbations. Luciano [26] further demonstrated that by increasing the magnitude of the perturbation, it is possible to achieve a transition even around $Re \approx 1000$. The authors conclude that the added perturbation in the simulation accounts for any small perturbations that always exists within the experiments. However, the physical grounds for such an assumption are disputable. Interestingly, Wygnanski and Champagne [27] observed that the enforcement of finite perturbations did not always ensure instability.

The authors note in passing that the conventional NS approach also struggles to explain the physical mechanism of drag reduction when a small amount of polymer molecules is added to a Newtonian solvent, as reported widely in the literature [28–34].

The difficulty of the classical NS theory to explain some of the experimentally observed transitions to turbulence led Volokh [35–37] to assume that considerations of purely kinematic instabilities of the laminar flow were not enough and material instabilities of the flow should also be taken into account. The latter extension of the NS theory can be done, for example, by the enforcement of finite viscous strength in the

* Corresponding author.
E-mail address: lahiriayan22@gmail.com (S.K. Lahiri).
[1] These authors contributed equally to this work.

https://doi.org/10.1016/j.rineng.2024.102535
Received 20 March 2024; Received in revised form 1 July 2024; Accepted 7 July 2024
Available online 10 July 2024

List of symbols

Re	Reynolds number	$\mathbf{D} = \frac{1}{2}\left(\text{grad}\mathbf{v} + \text{grad}\mathbf{v}^{\mathrm{T}}\right)$	Symmetric strain rate tensor
$\mathbf{v}$	Flow velocity	ρ	Fluid (water) density
D	Diameter of the pipe	η	Viscosity
L	Length of the pipe	ϕ	Critical strain rate
m	VSM parameter	η^*	Generalized viscosity
v_{in}	Peak inlet velocity	τ	Shear stress
		τ_{cr}	Critical shear stress

constitutive law. Physically, it means that viscosity drops at the critical strain rate because internal friction breaks down leading to instability of the laminar flow. The viscous stress corresponding to the critical strain rate is termed the viscous strength of the fluid. It is a material property.

Quite amazingly, the recent molecular dynamic simulations by Raghavan and Ostoja-Starzewski [38] confirm the assumption of viscous strength in the continuum mechanics formulation.

Despite its theoretical promise and some analytical results [35–37], the proposed modified NS constitutive model with viscous strength was not examined in specific numerical simulations of a three-dimensional pipe flow. This gap is filled in the present work. Results of numerical simulations are reported below, which show the transition to turbulence in the pipe flow with the modified NS approach. This transition is due to the process of growing material instabilities.

2. Navier-Stokes model enhanced with viscous strength

To summarize the governing equations of pipe flow, the linear momentum balance in the standard form can be presented as

$$\rho\frac{\partial \mathbf{v}}{\partial t} + \rho(\text{grad}\mathbf{v})\mathbf{v} = -\text{grad}p + \text{div}\boldsymbol{\tau}, \tag{1}$$

where ρ is the mass density; $\mathbf{v}$ is the velocity obeying the incompressibility condition $\text{div}\mathbf{v} = 0$; t is time; p is the hydrostatic pressure; and $\boldsymbol{\tau}$ is the viscous stress tensor.

The governing equations also include the constitutive law. For Newtonian fluids, the viscous stress is proportional to the strain rate

$$\boldsymbol{\tau} = 2\eta\mathbf{D}, \tag{2}$$

where η is the fluid viscosity and $\mathbf{D} = \left(\text{grad}\mathbf{v} + \text{grad}\mathbf{v}^{\mathrm{T}}\right)/2$ is the strain rate tensor equal to the symmetric part of the velocity gradient.

In the viscous strength model [35], a finite strain rate limiter is incorporated in the viscosity function that remains constant until a critical point, beyond which the viscosity drops to zero representing a breakdown of contacts between fluid layers

$$\eta^* = \eta\exp\left[-\left(\frac{\mathbf{D}:\mathbf{D}}{\phi^2}\right)^m\right], \tag{3}$$

where $\mathbf{D}:\mathbf{D} = \text{tr}\left[\mathbf{D}\mathbf{D}^{\mathrm{T}}\right]$ is the squared equivalent scalar strain rate; m is a constant; and ϕ is the critical equivalent strain rate, which is a saturation limit for the material stability of the fluid.

The viscosity function has essentially two modes – nonzero constant, which describes a classical Newtonian fluid, and zero constant, corresponding to the ideal fluid with negligible internal friction:

$$\eta^* = \begin{cases} \eta & \text{when } \mathbf{D}:\mathbf{D} < \phi^2 \\ 0 & \text{when } \mathbf{D}:\mathbf{D} > \phi^2, \end{cases} \tag{4}$$

By increasing the magnitude of constant m in Eq. (3), it is possible to approach the step function that physically means a breakdown in the internal friction between fluid layers – Fig. 1a.

Accordingly, the modified constitutive model incorporating the viscous strength becomes

$$\boldsymbol{\tau} = 2\eta^*\mathbf{D}. \tag{5}$$

For the sake of clarification, let us consider shear flow with nonzero strain rate component D_{xy} and stress τ_{xy}. In this case, the constitutive law takes the form

$$\frac{\tau_{xy}}{\eta\phi} = 2\left(\frac{D_{xy}}{\phi}\right)\exp\left[-2^m\left(\frac{D_{xy}}{\phi}\right)^{2m}\right]. \tag{6}$$

Its graphical representation in Fig. 1b shows that, unlike the classical NS theory, the shear stress possesses a finite limit – strength – indicating the breakdown of internal viscous friction. The strain rate corresponding to this stress bound can be obtained by solving $d\tau_{xy}/dD_{xy} = 0$ for Eq. (6), which results in

$$\frac{D_{xy}}{\phi} = \left[\frac{1}{2^{m+1}\,m}\right]^{\frac{1}{2m}}. \tag{7}$$

Hence, the viscous strength of the fluid becomes $\tau_{xy} = \sqrt{2}\eta\phi$ for $m \gg 1$.

Remark 1. The authors note that the conventional Navier-Stokes assumption of the perfectly intact viscous bonds is an extreme case of the viscous strength model with $\phi \to \infty$. In other words, the traditional NS model has infinitely large viscous strength. The latter means that friction between adjacent fluid layers is always ideal and the viscous stress can increase infinitely with the increasing strain rate. Such property of the NS model is doubtful on physical grounds because no unbreakable materials really exist.

Remark 2. The model parameter m helps in the mathematical smoothing of the step function. For materials with finite viscous stress, the critical strain rate can be obtained with the help of equality $\lim_{m\to\infty}\left[\frac{1}{2^{m+1}\,m}\right]^{\frac{1}{2m}} = \frac{1}{\sqrt{2}}$.

3. Pipe flow simulations

In this section, the authors describe simulations of a three-dimensional pipe flow through a 60 mm long perfectly straight cylindrical pipe with a uniform circular cross section of diameter $D = 4$ mm; see Fig. 2a. The authors used two material models:

(a) Conventional Navier-Stokes model with infinite viscous strength, further abbreviated CV;
(b) Modified Navier-Stokes model with finite viscous strength, further abbreviated VSM.

The fluid is water with mass density $\rho = 1000$ kg/m^3, viscosity $\eta = 0.001$ kg/m/s, critical equivalent strain rate [35,36] $\phi = 848.5$ s^{-1}, and constant $m = 20$. For the sake of comparison, specific sections are chosen in the pipe (see Fig. 2b) to record measurements of respective simulations.

The accuracy of a numerical solution is highly influenced by the chosen discretization scheme. In our case studies, we anticipate local instabilities as fluid layers lose internal friction beyond the critical strain

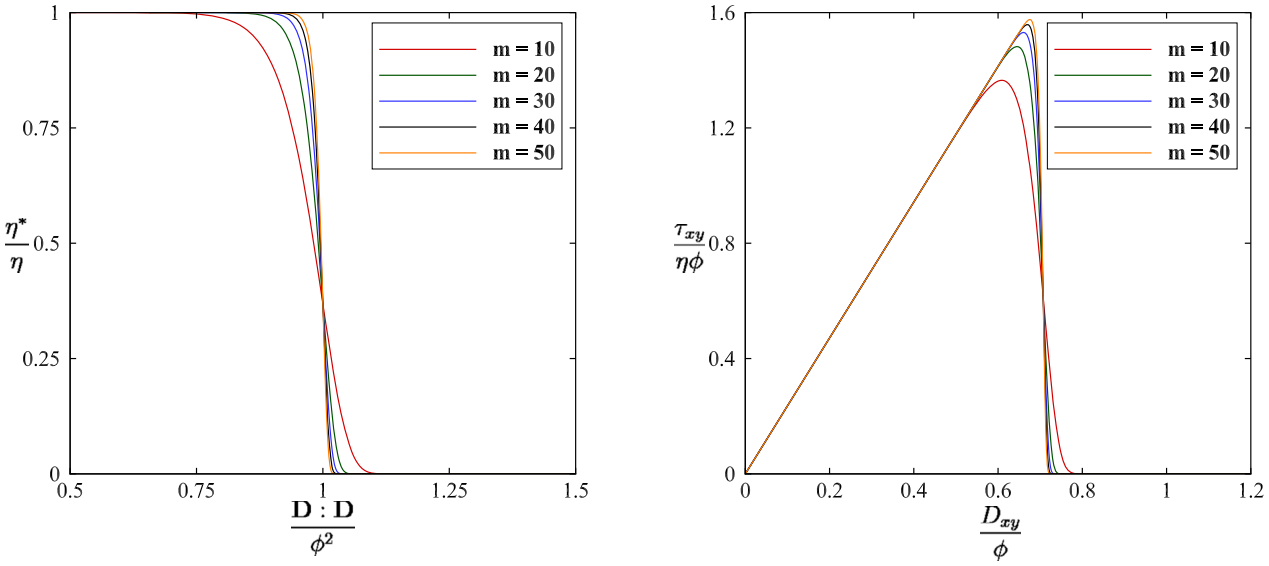

(a) viscosity versus equivalent strain rate

(b) stress versus strain rate

Fig. 1. Viscous strength model.

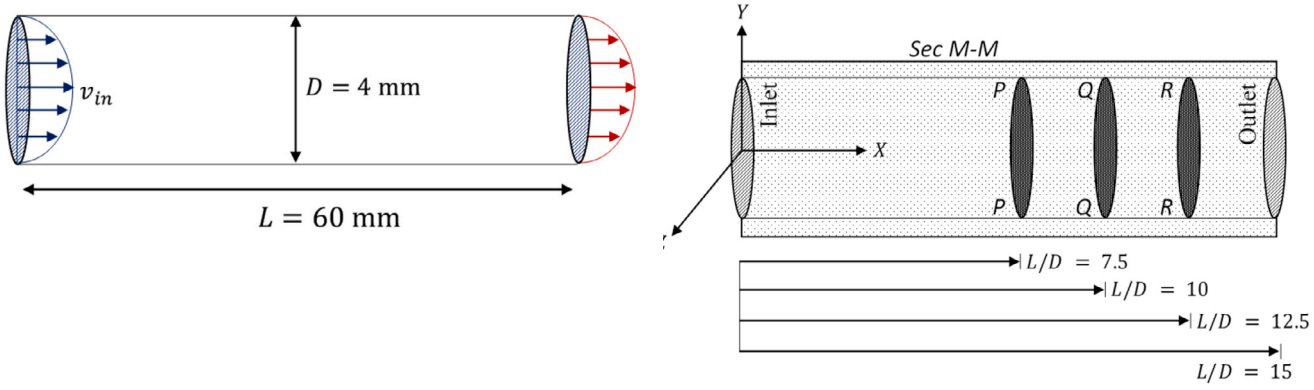

(a) Three-dimensional flow through a cylindrical pipe

(b) Section cut at specific locations in the pipe for recording and comparison of numerical results

Fig. 2. Schematic diagram of the problem.

rate, leading to a significant drop in shear stress (see Fig. 1b). For problems involving regions with sharp gradients, structured grids suffer from a higher numerical diffusion. In such cases, unstructured meshes offer superior adaptability to local solution variations, ensuring precise representation of significant changes. This choice is crucial to achieve more accurate solutions in areas with rapid changes or sharp gradients.

The authors utilize the unstructured mesh discretization in the commercial software ANSYS-R1. Fig. 3 illustrates the discretization at a typical pipe cross-section. The boundary conditions and assumptions are as follows:

- Inlet:: initially stable and, hence, a fully developed parabolic flow profile (Fig. 4)
- Outlet:: Zero pressure boundary condition
- Pipe Wall:: stationary with no-slip boundary conditions

Numerous computational studies [39–42] on turbulent pipe flow simulations indicate that assuming a uniform velocity condition at the inlet face leads to velocity overshoot. To address this, the authors adopted a stable parabolic inlet velocity condition, aligning with the

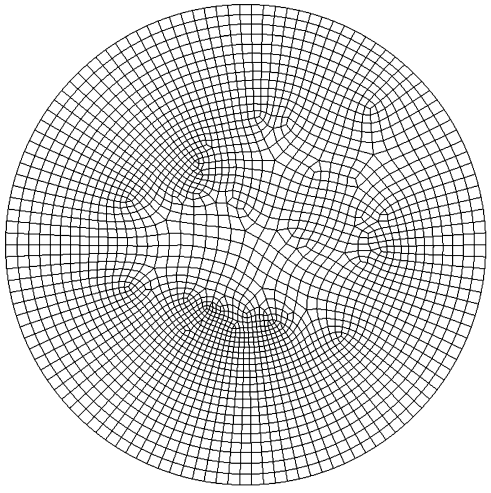

Fig. 3. Typical cross-sectional mesh.

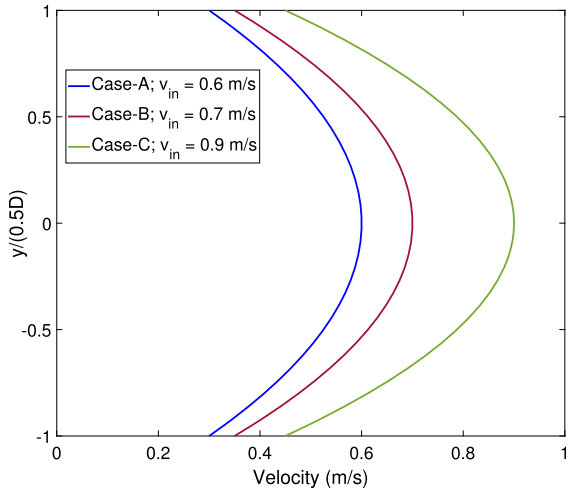

Fig. 4. Velocity profiles provided at the inlet of the pipe for different simulation cases.

Table 1
Inlet velocity (v_{in}) and Reynolds number (Re) for different load cases ($\rho = 1000$ kg/m^3; $D = 4$ mm; $\eta = 0.001$ kg/m/s).

Load case	Inlet velocity (v_{in}) (m/s)	$Re = \frac{2\rho v_{\text{in}} D}{3\eta}$
A	0.6	1600
B	0.7	1867
C	0.9	2400

no-slip boundary condition at the pipe wall. The Reynolds number can be approximated by relating the peak inlet velocity to a uniform velocity $\hat{v}$, which generates a fully developed velocity profile at the inlet face, as shown in Fig. 4. According to laminar flow theory, the relationship between $\hat{v}$ and v_{in} is given by $\hat{v} = \frac{2v_{\text{in}}}{3}$, resulting in a Reynolds number $Re = \frac{2\rho v_{\text{in}} D}{3\eta}$. To capture the transition, numerical simulations were conducted for three load cases by varying the peak inlet velocity v_{in}. Specifying the inlet velocity provides a clear understanding of the velocity gradient generated within the flow. Table 1 lists the peak inlet velocities and the corresponding Reynolds numbers for all the loading cases considered in the numerical examples.

The choice of an appropriate numerical framework is essential to capture the underlying physical processes governing the genesis of material instability in a pipe flow problem. For realistic 3D flows, the direct numerical solution becomes intractable. Instead, the large Eddy simulation (LES) is routinely used to save time. The specific advantage of LES lies in effectively reducing computational costs, yet capturing the transition to turbulence with reasonable accuracy. The LES filters out small-scale eddies, insignificant to turbulence, from the solution and determines the unknowns using a subgrid turbulence model. Among various subgrid turbulence models [43–47] reported in the literature, the wall-adopted local eddy-viscosity (WALE) [45] approach is advantageous for problems related to transitional flows. In principle, the WALE model represents proper scaling at the wall functions and returns a zero turbulent eddy viscosity (μ_{t}) for laminar shear flows, which makes it appropriate to treat laminar zones in the fluid domain.

Remark 3. The accuracy of any computational model is sensitive to the choice and level of discretization of the problem domain. The authors conducted a grid independence study for velocity test case I; i.e. $v_{\text{in}} = 0.6$ m / s, i.e. $Re \approx 1600$ with three different sets of mesh size discretization 0.3 mm (769186 elements), 0.1 mm (1514833 elements), and 0.08 mm (2998621 elements). However, the convergence study is only limited to

Table 2
Y^+ value in VSM simulation for velocity case I: $v_{\text{in}} = 0.6$ m / s i.e. $Re \approx 1600$.

Mesh size (mm)	No of nodes	Y^+
0.3	769186	5.2 - 14
0.1	1514833	0.88 - 1.12
0.05	2998621	0.04 - 0.76

$re \approx 1600$. Further to ensure a proper and accurate wall treatment near the pipe wall the authors carefully studied the corresponding maximum Y^+ values for each set of simulations (Table 2). The authors chose the optimum discretization mesh size of 0.1 mm (1514833 elements) for rest of the simulations.

In the first set of simulations, with the peak inlet velocity of $v_{\text{in}} = 0.6$ m/s i.e. $Re \approx 1600$ (refer to Table 1) the CV model (i.e. the classical NS model with infinite viscous strength) predicts a stable laminar flow; whereas in the VSM (i.e. the modified NS model with finite viscous strength) the authors can observe instability in the flow. This highly localized material instability triggers deviation from laminar flow near the outlet of the pipe (Fig. 5a). The onset of instability is visible in the profile of the longitudinal velocity across the cross section of the pipe at a distance $L/D = 10$ from the inlet face (section Q-Q in Fig. 2b) of the pipe (Fig. 5b).

As the authors increase the inlet velocity to $v_{\text{in}} = 0.7$ m / s, i.e., $Re \approx 1867$, the CV model still predicts a perfectly stable solution and the flow remains perfectly laminar. However, in the VSM solution the authors can observe a visible deviation from the laminar flow pattern (Fig. 5c). In this case, the instabilities are more pronounced than the first case. The contour of longitudinal velocity across the cross-section of the pipe at a distance $L = 10D$ (section Q-Q in Fig. 2b) in Fig. 5d demonstrates a clear transition to turbulence.

With the further increase in the inlet velocity to $v_{\text{in}} = 0.9$ m/s, that is, $Re \approx 2400$, the VSM simulation produces a turbulent flow with eddies spread globally along the length of the pipe (Fig. 5e) while the CV model still provides a stable laminar flow. Like in the previous examples, in section Q-Q, $L = 10D$ distant from the inlet, Fig. 5f indicates complete loss of the laminar mode in the longitudinal flow.

Instabilities in the flow generate localized puffs or fluctuations in the transverse velocity profile in the channel. The VSM simulation reports that the peak fluctuation is ≈ 0.1 m/s, whereas for the CV model the authors do not notice any significant fluctuation for $v_{\text{in}=0.6}$ m/s (Figs. 6a-6b). These fluctuations are highly localized in nature and the flow remains laminar. As the authors increase the inlet velocity to $v_{\text{in}=0.7}$ m / s, the localized puffs magnify and the peak magnitude reaches ≈ 0.16 m/s (Figs. 7a-7b). For $v_{\text{in}} = 0.9$ m/s, that is, $Re \approx 2400$, the VSM simulation yields a turbulent flow with eddies with a maximum variation in the transverse velocity of ≈ 0.25 m/s (refer to Figs. 8a-8b).

Remark 4. The authors note that the standard viscometer/rheometer tests are useless for the calibration of fluid strength. In fact, to observe the drop in viscosity, all fluid particles should reach the critical state simultaneously. That is practically impossible and the viscosity drops randomly at some points where the local material instability develops. Thus, only the observation of the onset of transition to chaos is suitable for calibration of the fluid strength. This issue is discussed with great attention in [36], to which the reader is referred.

Remark 5. The authors again emphasize that the authors used the same techniques for large-eddy simulations for both the classical Navier-Stokes model and the model enhanced with strength. The latter model presents viscosity as a step function with nonzero and zero viscosity coefficients. The theory of large-eddy simulations is equally applicable to both constitutive models and the comparison of the results is objective.

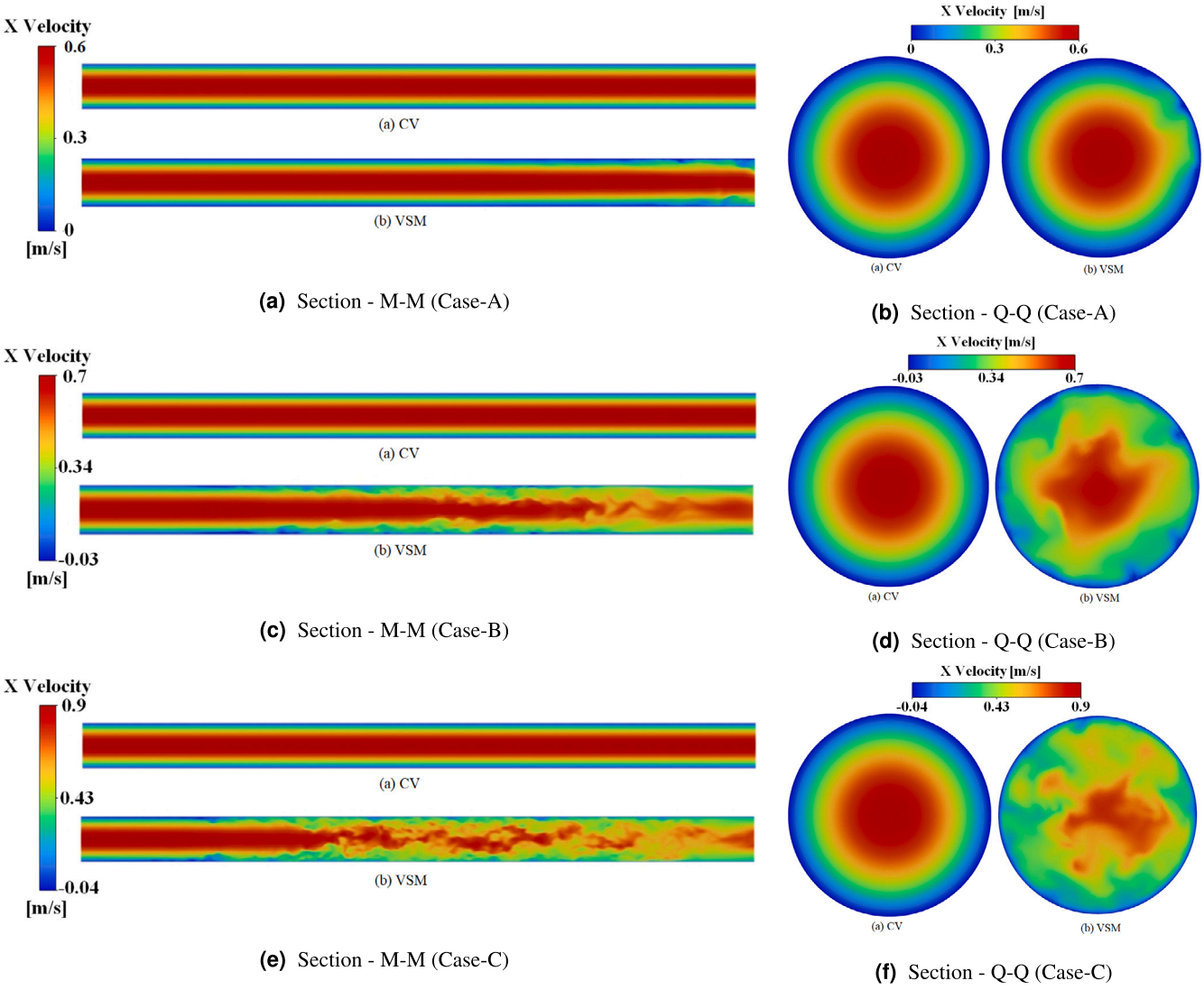

Fig. 5. Variation of flow velocity (v_x) (refer to sections M-M, and Q-Q in Fig. 2b) for different inlet velocity conditions — A, B, & C (Table 1).

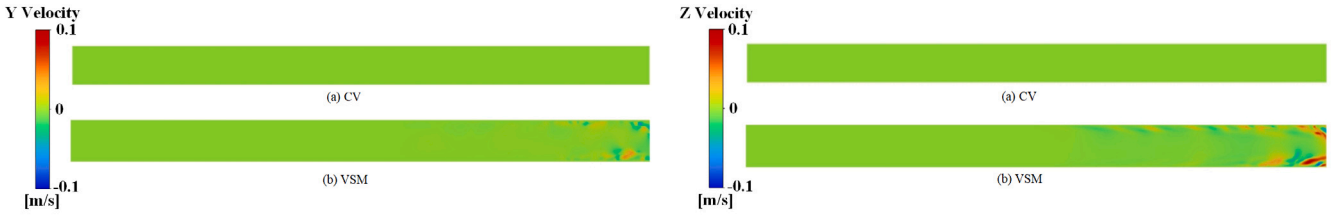

Fig. 6. Variation of transverse velocity along the length of the pipe at section M-M (refer to Fig. 2b) for inlet velocity case A ; $v_{\text{in}=0.6m/s}$.

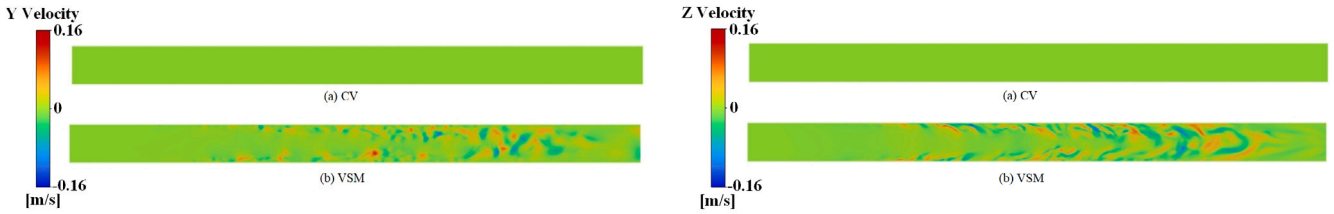

Fig. 7. Variation of transverse velocity along the length of the pipe at section M-M (refer to Fig. 2b) for inlet velocity case B ; $v_{\text{in}=0.7m/s}$.

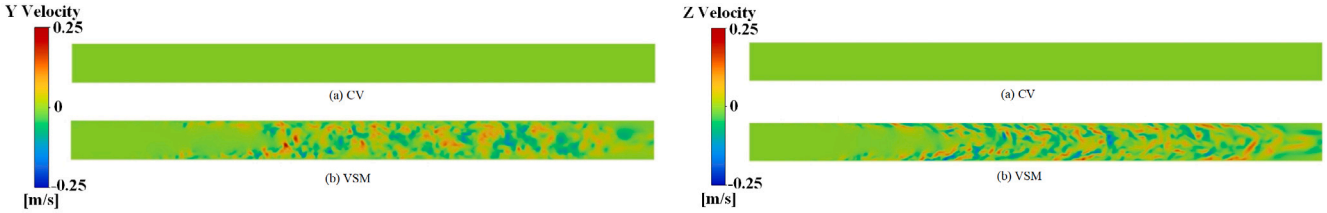

(a) Velocity in y-y direction v_y **(b)** Velocity in z-z direction v_z

Fig. 8. Variation of transverse velocity along the length of the pipe at section M-M (refer to Fig. 2b) for inlet velocity case C ; $v_{\text{in}=0.9m/s}$.

Table 3
Maximum strain rate and wall shear stress in the channel section for the CV model or conventional Navier-Stokes equation under different inlet velocity conditions ($\phi = 848.5\ s^{-1}$).

	Inlet velocity	Max strain rate	Max wall shear	
Case	(v_{in})	($\sqrt{\mathbf{D}:\mathbf{D}}$)	(τ_{max})	$\frac{\sqrt{\mathbf{D}:\mathbf{D}}}{\phi}$
	m/s	s^{-1}	Pa	
A	0.6	596.7	0.60	0.70
B	0.7	696.2	0.71	0.82
C	0.9	895.2	0.91	1.06

4. Discussion

Based on the numerical simulations reported above, the authors suggest that the turbulence is an outcome of two main events: the genesis of material instabilities in the laminar flow and the transition and growth of local instabilities in large eddies. Instabilities appear initially due to the reduction in viscous stresses with the increase in flow strain rates.

Our simulations and some parameters collected in Table 3 prompt that material instabilities are born at $v_{\text{in}} = 0.6$ m/s. The latter means that shear stresses begin to drop near the pipe wall, small eddies appear and begin to grow, and the flow deviates from the laminar (Fig. 9a; Case-A) behavior. When the flow velocity increases to $v_{\text{in}} = 0.7$ m/s, the fluid remains within the transition range, but the instabilities and eddies expand over a wider zone (Fig. 9a; Case-B). By increasing the inlet velocity to $v_{\text{in}} = 0.9$ m/s (Case-C), the eddies become large and spread throughout the pipe (Fig. 9a; Case-C).

Once the instability arises, the drop in the shear stress near the zone of instability induces disturbances in transverse velocities. The magnitude of the disturbances increases with increasing flow velocity (Figs. 9b-9c). The turbulence moves towards the inlet face of the pipe with an increase in the inlet velocity of the fluid. The variation in axial velocity in section M-M is marginal for $v_{\text{in}} = 0.6$ m/s.

Fig. 10 presents another interesting phenomenon: as the fluid loses its stability, the strain rates are magnified near the zone of instability. Subsequently, during the transition to turbulence, the magnified strain rates start propagating towards the center of the pipe.

The flow profiles generated in the simulations demonstrate the ability of the constitutive model to capture the developing turbulence. The initial visible sign of instability originates in Case-A at a distance of $L = 10D$ from the inlet face of the pipe (Fig. 11a). As the inlet velocity increases to 0.7 m/s and 0.9 m/s in Case-B and Case-C respectively, the local instability diffuses towards the inlet face resulting in turbulence much closer to the inlet (Figs. 11b-11c). While in Fig. 11a the flow remains laminar up to $L = 12.5D$ from the inlet, the laminar zone is predominantly restricted up to $L = 7.5D$ in Fig. 11b. A further increase in the inlet velocity makes the flow turbulent even before $L = 7.5D$ - Fig. 11c.

5. Conclusions

In this study, numerical simulations of pipe flow based on the Navier-Stokes model with and without viscous strength were conducted. The main conclusions drawn from the simulations are:

- The modified Navier-Stokes model incorporating the viscous strength can capture transition from laminar to turbulent regime in pipe flow, whereas the classical Navier-Stokes model without the viscous strength fails to do that.
- The simulations suggest that the local instabilities originate at $Re \approx 1600$ and subsequently grow into globally chaotic turbulent motion at $Re \approx 2400$, which corresponds well with the recent experimental observations reported by Avila et al. [6].
- The viscous strength model does not require any ad-hoc perturbation to be included in the numerical simulation.

The authors hypothesise that material and kinematic instabilities both play a role in the transition from laminar to turbulent flows. Introduction of the material parameter of viscous strength is a possible way to enforce material instabilities in the constitutive models of fluids. Such instabilities can trigger transitions to chaotic flow when kinematic instabilities are absent. Enhancing the classical Navier-Stokes model with a finite viscous strength parameter offers new opportunities to simulate and understand the transition to turbulence. To elaborate the capacity of the viscous strength model, the present work is concentrated only on perfectly straight Newtonian pipe flow simulations. The modified constitutive model can be used in simulations of various flows with possible transition to turbulence in the future.

CRediT authorship contribution statement

Saptarshi Kumar Lahiri: Writing – original draft, Visualization, Validation, Software, Formal analysis. **Konstantin Volokh:** Writing – review & editing, Resources, Funding acquisition, Conceptualization.

Declaration of competing interest

The authors declare the following financial interests/personal relationships which may be considered as potential competing interests: Konstantin Volokh reports financial support was provided by Israel Science Foundation (ISF 394/20). If there are other authors, they declare that they have no known competing financial interests or personal relationships that could have appeared to influence the work reported in this paper.

Data availability

Data will be made available on request.

Acknowledgements

This work was supported by The Israel Science Foundation (ISF-394/20).

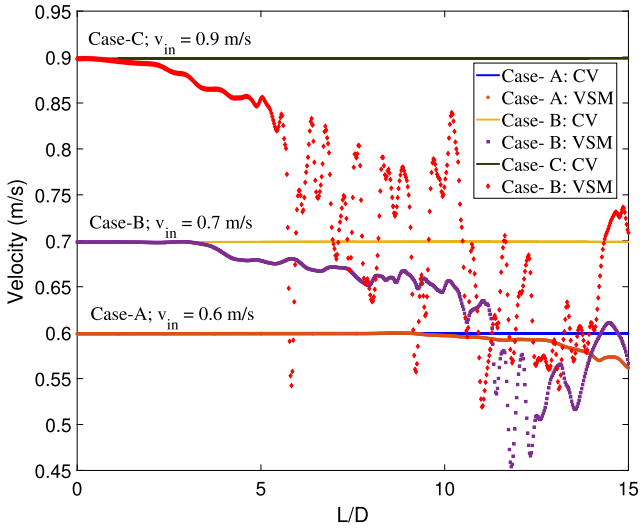

(a) Profile of longitudinal velocity v_x

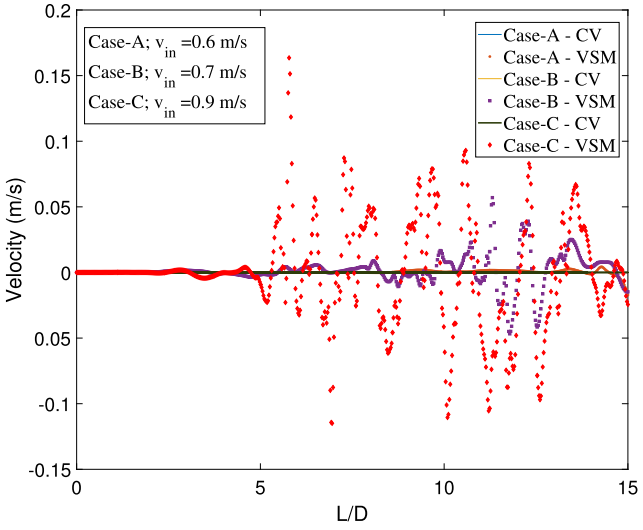

(b) Profile of transverse velocity v_y

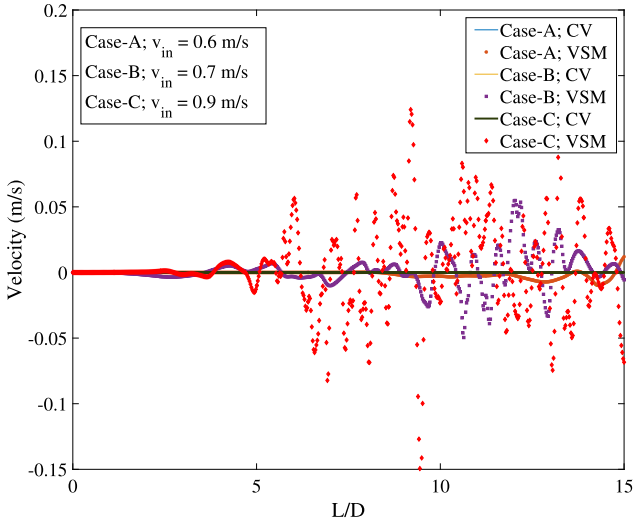

(c) Profile of transverse velocity v_z

Fig. 9. Variation in flow velocities along the direction of pipe flow at section M-M (cut at the midplane where $z = 0$, refer to Fig. 2b) for velocity cases A, B, and C.

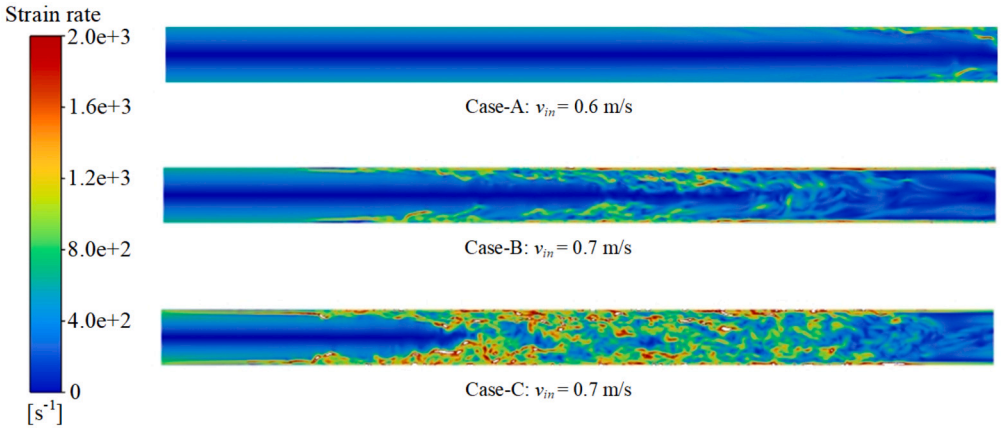

Fig. 10. Magnification of the strain rate ($\sqrt{\mathbf{D} : \mathbf{D}}$) in the M-M section (at $z = 0$, in Fig. 2b) for different inlet velocity conditions — Case – A,B, & C.

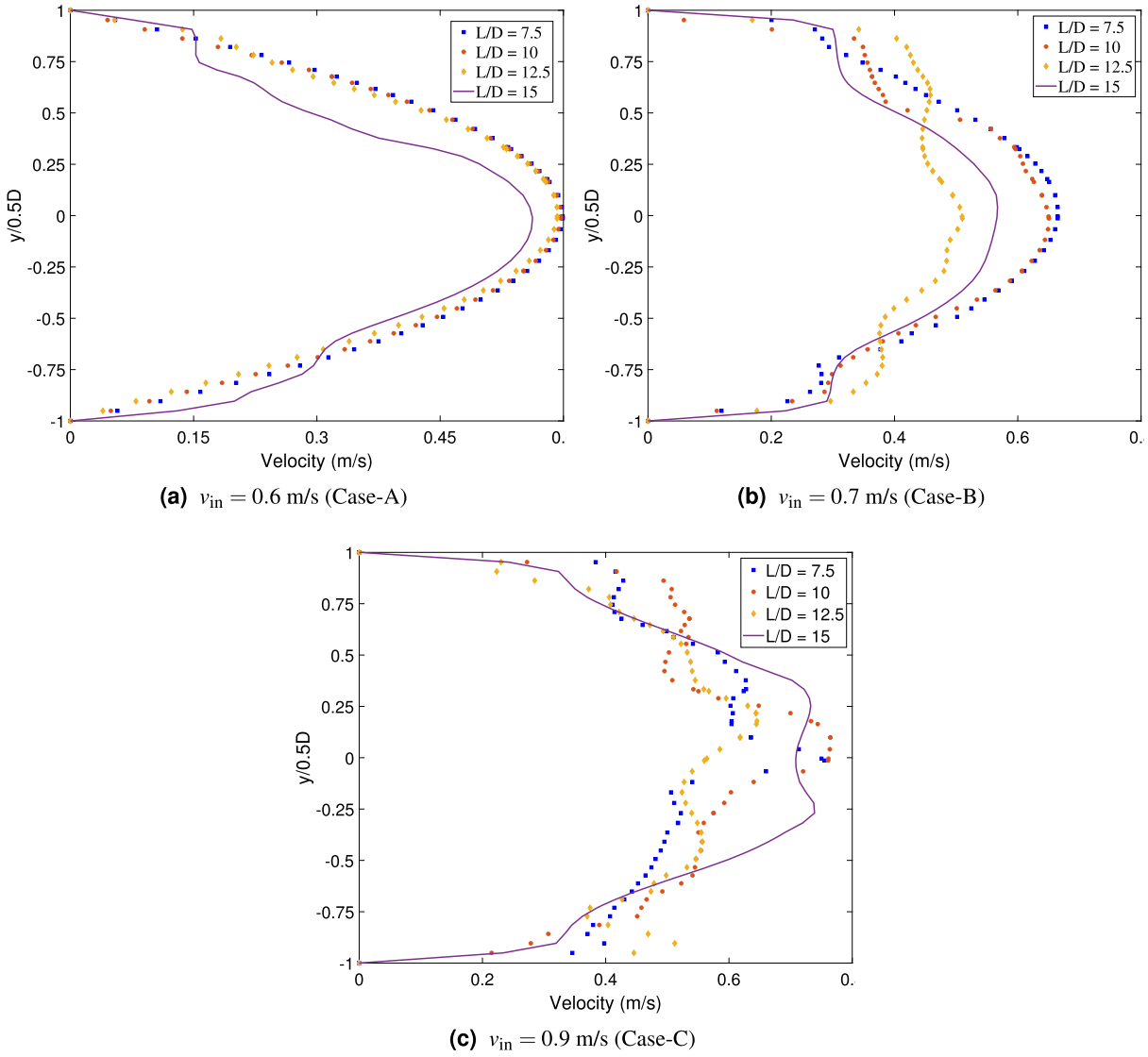

(a) $v_{\text{in}} = 0.6$ m/s (Case-A)

(b) $v_{\text{in}} = 0.7$ m/s (Case-B)

(c) $v_{\text{in}} = 0.9$ m/s (Case-C)

Fig. 11. Variation of longitudinal velocity (v_x) across the cross-section of the pipe cut at distances L = 7.5D, 10D, 12.5D, and 15D downstream from the inlet face (*refer to cross-sections P-P, Q-Q, R-R, and outlet* in Fig. 2b) for different inlet velocity conditions.

References

[1] O. Reynolds, An experimental investigation of the circumstances which determine whether the motion of water shall be direct or sinuous, and of the law of resistance in parallel channels, Philos. Trans. R. Soc. Lond. (1883) 935–982.

[2] O. Reynolds, On the dynamical theory of incompressible viscous fluids and the determination of the criterion, Philos. Trans. R. Soc. Lond. (1895) 123–164.

[3] H. Faisst, B. Eckhardt, Sensitive dependence on initial conditions in transition to turbulence in pipe flow, J. Fluid Mech. 504 (2004) 343–352.

[4] B. Eckhardt, Turbulence transition in pipe flow: some open questions, Nonlinearity 21 (2007) T1.

[5] B. Eckhardt, Introduction. Turbulence transition in pipe flow: 125th anniversary of the publication of Reynolds' paper, Philos. Trans. - Royal Soc., Math. Phys. Eng. Sci. 367 (2009) 449–455.

[6] K. Avila, et al., The onset of turbulence in pipe flow, Science 333 (2011) 192–196.

[7] J.P. Gollub, H.L. Swinney, Onset of turbulence in a rotating fluid, Phys. Rev. Lett. 35 (1975) 927.

[8] M.J. Feigenbaum, Quantitative universality for a class of nonlinear transformations, J. Stat. Phys. 19 (1978) 25–52.

[9] R.I. Tanner, K. Walters, Rheology: An Historical Perspective, Elsevier, 1998.

[10] P. Manneville, On the transition to turbulence of wall-bounded flows in general, and plane Couette flow in particular, Eur. J. Mech. B, Fluids 49 (2015) 345–362.

[11] P. Manneville, Transition to turbulence in wall-bounded flows: where do we stand?, Mech. Eng. Rev. 2 (2016) 15–00684.

[12] D. Barkley, Theoretical perspective on the route to turbulence in a pipe, J. Fluid Mech. 803 (2016).

[13] M. Eckert, The Turbulence Problem. A Persistent Riddle in Historical Perspective, Springer, 2019.

[14] M. Eckert, Turbulence—an Odyssey. Origins and Evolution of a Research Field at the Interface of Science and Engineering, Springer, 2022.

[15] M. Avila, D. Barkley, B. Hof, Transition to turbulence in pipe flow, Annu. Rev. Fluid Mech. 55 (2023) 575–602.

[16] V.A. Romanov, Stability of plane-parallel Couette flow, Funct. Anal. Appl. 7 (1973) 137–146.

[17] L.D. Landau, E.M. Lifshitz, Fluid Mechanics, vol. 6, Elsevier, 2013.

[18] J. Peixinho, T. Mullin, Decay of turbulence in pipe flow, Phys. Rev. Lett. 96 (2006) 094501.

[19] E. Sanmiguel-Rojas, C. Del Pino, C. Gutiérrez-Montes, Global mode analysis of a pipe flow through a 1: 2 axisymmetric sudden expansion, Phys. Fluids 22 (2010).

[20] K.A. Cliffe, E.J. Hall, P. Houston, E.T. Phipps, A.G. Salinger, Adaptivity and a posteriori error control for bifurcation problems III: incompressible fluid flow in open systems with o (2) symmetry, J. Sci. Comput. 52 (2012) 153–179.

[21] E. Sanmiguel-Rojas, T. Mullin, Finite-amplitude solutions in the flow through a sudden expansion in a circular pipe, J. Fluid Mech. 691 (2012) 201–213.

[22] K. Selvam, J. Peixinho, A.P. Willis, Localised turbulence in a circular pipe flow with gradual expansion, J. Fluid Mech. 771 (2015) R2.

[23] K. Selvam, J. Peixinho, A.P. Willis, Flow in a circular expansion pipe flow: effect of a vortex perturbation on localised turbulence, Fluid Dyn. Res. 48 (2016) 061418.

[24] N. Moallemi, J. Brinkerhoff, Instability and localized turbulence associated with flow through an axisymmetric sudden expansion, Int. J. Heat Fluid Flow 72 (2018) 161–173.

[25] D. Vittal Shenoy, M. Safdari Shadloo, J. Peixinho, A. Hadjadj, Direct numerical simulations of laminar and transitional flows in diverging pipes, Int. J. Numer. Methods Heat Fluid Flow 30 (2020) 75–92.
[26] R.D. Luciano, X. Chen, D. Bergstrom, Discretization and perturbations in the simulation of localized turbulence in a pipe with a sudden expansion, J. Fluid Mech. 935 (2022) A20.
[27] I.J. Wygnanski, F. Champagne, On transition in a pipe. Part 1. The origin of puffs and slugs and the flow in a turbulent slug, J. Fluid Mech. 59 (1973) 281–335.
[28] B.A. Toms, Some observations on the flow of linear polymer solutions through straight tubes at large Reynolds numbers, in: Proceedings of the First International Congress on Rheology 2, 1949, pp. 135–141.
[29] A. Boelens, M. Muthukumar, Rotational relaxation time as unifying time scale for polymer and fiber drag reduction, Phys. Rev. E 93 (2016) 052503.
[30] H.-W. Bewersdorff, Drag Reduction of Turbulent Flows by Additives, Kluwer, 1995.
[31] R.H. Nadolink, W.W. Haigh, Bibliography on skin friction reduction with polymers and other boundary-layer additives, Appl. Mech. Rev. 47 (1995) 351–460.
[32] P. Ptasinski, et al., Turbulent channel flow near maximum drag reduction: simulations, experiments and mechanisms, J. Fluid Mech. 490 (2003) 251–291.
[33] L. Xi, X. Bai, Marginal turbulent state of viscoelastic fluids: a polymer drag reduction perspective, Phys. Rev. E 93 (2016) 043118.
[34] J.L. Lumley, Drag reduction by additives, Annu. Rev. Fluid Mech. 1 (1969).
[35] K. Volokh, An investigation into the stability of a shear thinning fluid, Int. J. Eng. Sci. 47 (2009) 740–743.
[36] K. Volokh, Navier-Stokes model with viscous strength, Comput. Model. Eng. Sci. 92 (2013) 87–101.
[37] K. Volokh, An explanation of the drag reduction via polymer solute, Acta Mech. 229 (2018) 4295–4301.
[38] B. Raghavan, M. Ostoja-Starzewski, Shear-thinning of molecular fluids in Couette flow, Phys. Fluids 29 (2017) 023103.
[39] P. Walklate, M. Heikal, A. Hatton, Measurement and prediction of turbulence and heat transfer in the entrance region of a pipe, Proc. Inst. Mech. Eng. 190 (1976) 401–407.
[40] F. Anselmet, et al., Axial development of the mean flow in the entrance region of turbulent pipe and duct flows, C. R., Méc. 337 (2009) 573–584.
[41] W. Kumara, B. Halvorsen, M. Melaaen, Computational study on non-asymptotic behavior of developing turbulent pipe flow, Adv. Fluid Mech. VIII 69 (2010) 39–52.
[42] D. Bryant, E.M. Sparrow, J.M. Gorman, Turbulent pipe flow in the presence of centerline velocity overshoot and wall-shear undershoot, Int. J. Therm. Sci. 125 (2018) 218–230.
[43] J. Smagorinsky, General circulation experiments with the primitive equations: I. The basic experiment, Mon. Weather Rev. 91 (1963) 99–164.
[44] M. Germano, U. Piomelli, P. Moin, W.H. Cabot, A dynamic subgrid-scale eddy viscosity model, Phys. Fluids A, Fluid Dyn. 3 (1991) 1760–1765.
[45] F. Nicoud, F. Ducros, Subgrid-scale stress modelling based on the square of the velocity gradient tensor, Flow Turbul. Combust. 62 (1999) 183–200.
[46] D.K. Lilly, A proposed modification of the germano subgrid-scale closure method, Phys. Fluids A, Fluid Dyn. 4 (1992) 633–635.
[47] M.L. Shur, P.R. Spalart, M.K. Strelets, A.K. Travin, A hybrid rans-les approach with delayed-des and wall-modelled les capabilities, Int. J. Heat Fluid Flow 29 (2008) 1638–1649.